Applied Catalysis B: Environmental 211 (2017) 205–211

Contents lists available at ScienceDirect

Applied Catalysis B: Environmental

journal homepage: www.elsevier.com/locate/apcatb

Research Paper

Synthesis of hierarchical platinum-palladium-copper nanodendrites for efficient methanol oxidation

Rong Chang[a], Lijun Zheng[a], Chengwen Wang[a], Dachi Yang[a,*], Gaixia Zhang[b], Shuhui Sun[b,*]

[a] Department of Electronics, College of Electronic Information and Optical Engineering, Nankai University, Tianjin 300350, People's Republic of China
[b] Institut National de la Recherche Scientifique-Énergie, Matériaux et Télécommunications, Université du Québec, Varennes QC J3X 1S2, Canada

ARTICLE INFO

Article history:
Received 5 December 2016
Received in revised form 6 March 2017
Accepted 12 April 2017
Available online 13 April 2017

Keywords:
Wet-chemistry
Nanodendrites
Nanowires
Methanol oxidation reaction (MOR)
Fuel cell

ABSTRACT

Tuning the architecture and composition of platinum (Pt)-based nanostructures for enhancing the electrocatalytic activity and stability towards methanol oxidation reaction (MOR) is pivotal for the commercialization of direct methanol fuel cells (DMFCs), but still remains great challenge. Here, hierarchical platinum-palladium-copper (PtPdCu) nanodendrites (NDs) with tip-cracked defects have been developed with tailored morphology and dopants. We firstly electrodeposited PtPdCu nanowires (NWs) inside the channels of aluminum anodic oxide (AAO) template, and then wet-chemically transformed the as-synthesized NWs into NDs. Benefiting from the synergetic effect between the tip-cracked defects and dopants, firstly, the MOR mass activity and specific activity of PtPdCu NDs are ~1.78 times and ~2.14 times higher than those of commercial Pt/C, respectively; secondly, after 2000 s stability test, the electrocatalytic activity of PtPdCu NDs is ~5.02 times higher than commercial Pt/C; finally, the PtPdCu NDs also show better CO tolerance as well. Our PtPdCu NDs are promising anode electrocatalysts in next-generation DMFCs.

1. Introduction

Direct methanol fuel cells (DMFCs) provide clean and high energy density power source, and hold great potential in portable electronic devices and small vehicle applications [1,2]. To fulfill the commercial implementation of DMFCs, a desirable highly efficient electrocatalyst towards methanol oxidation reaction (MOR) is required to be cheap, highly active and stable. Currently, Pt and Pt-based catalysts still remain the research focus. Basically, transition metals (Ru, Co, Fe, Cu and Ni) are doped into Pt nanostructures to modify its "d-band" for achieving improved catalytic performance [3,4]. However, it is known that Pt catalysts are prone to be poisoned by intermediate carbonaceous and sulfur-containing species during organic molecule oxidation [5]. By comparison, palladium (Pd), with similar electronic structure (*fcc* structure) to Pt, is more abundant [6], less expensive and also active for MOR [7]. Additionally, studies suggest that Pt-Pd alloy catalyst [8] can conspicuously reduce Pt loading without lowering the catalytic activity and also provide a visible route for reducing CO poisoning effect [9] by weakening its surface concentration.

Surface defect sites, including kinks, steps and edges with lower coordination numbers, are known to be both more adsorptive and more reactive than flat surface [10]. Moreover, because the d-band of Pt becomes narrower and shifts upward closer to the Fermi level [11], the altered electronic structure of Pt results in a higher oxophilicity [12] at defect sites. By elevating the density of defects, the MOR activity is also able to be improved by several orders of magnitude [13,14]. Meanwhile, surface defects provide the feasibility in improving CO tolerance. For example, if there were Pt atoms situated at edge sites employed towards MOR, the onset potential of CO oxidation will occur as low as 0.16 V [15]. To date, porous nanostructures have been widely investigated owing to not only providing such defects, but also improving the utilization of Pt by exposing more inner Pt atoms as active sites. Accordingly, to obtain such porous nanostructures with desired compositions (e.g., overall, surface and bulk ratios of metal A and B), geometry and crystalline (e.g., size, shape and crystal facets) configurations, numerous synthesis strategies have been developed [16–19]. Despite great progress, either complicated procedures or critical facilities are involved, the synthetic art on the nanostruc-

* Corresponding authors.
E-mail addresses: yangdachi@nankai.edu.cn (D. Yang), shuhui@emt.inrs.ca (S. Sun).

http://dx.doi.org/10.1016/j.apcatb.2017.04.040
0926-3373/

tures that are decorated with desired surface defects needs further exploring.

Hierarchical structures that are constructed by low dimensional nanomaterials, have attracted extensive attention owing to not only maintaining large surface-to-volume (s/v) ratio but also avoiding the dissolution and Ostwald ripening/aggregation [20,21] of zero-dimensional (0D) Pt nanoparticles. Therefore, an ideal strategy may be proposed to design hierarchical PtPdCu alloy electrocatalysts with synergetic effect on Cu creating tip-cracked defects to guarantee high utilization of Pt and improve CO tolerance, meanwhile, with Pt maintaining excellent activity and Pd reducing CO poisoning effect. Such a desirable catalyst towards MOR is highly advantageous, unfortunately, generic synthesis art is still challenging.

Here, PtPdCu nanodendrites (NDs) with "tip-cracks" and hierarchical shapes have been developed, via first electrodeposition of cylindrical PtPdCu nanowires (NWs) arrays inside the channels of AAO template, followed by a wet-chemical modification, as is schematically illustrated in Fig. 1. In our synthesis, Cu works as intermediate for the NWs-NDs transformation, and also contributes to the morphology tailoring process of the NWs. The enhanced MOR performance is benefited from the synergetic effect between the dendritic morphology and Pd dopants. The mass activity and stability of the PtPdCu NDs are evaluated to be ~1.78 and ~5.02 times higher than those of the commercial 20 wt% Pt/C catalyst, respectively. Additionally, the tip-cracked PtPdCu NDs possess an enhanced CO tolerance.

2. Experimental

2.1. Preparations of the PtPdCu NDs

The PtPdCu NWs arrays were prepared by a conventional AAO template-confined synthesis [18,22]. Typically, the electrolyte contained 2.5 mM $H_2PtCl_6{\cdot}6H_2O$, 1.25 mM $PdCl_2$, 0.625 mM $CuCl_2{\cdot}2H_2O$, 0.5 mM H_3BO_3, was buffered to pH = 4 with HCl and NaOH. The AAO templates (~70 nm in pore diameter) were prepared similar to the previous work [23,24]. A thick Au layer was sputtered onto either side of the AAO templates to block the pores completely serving as the working electrode. A two-electrode system with the applied constant voltage of 2.0 ~ 2.5 V was utilized to carry out electrodeposition. The as-prepared PtPdCu NWs were first released from the AAO template in 4 M NaOH, and were then rinsed thoroughly with deionized water. An etching solution of 0.1 M HNO_3 was utilized to partially etch the Cu off the PtPdCu NWs for 1 h at 50 °C, and the samples were rinsed thoroughly with deionized water.

2.2. Characterizations

After being completely dried, the samples were characterized by X-ray diffraction (XRD), field-emission scanning electron microscopy (FE-SEM, JEOL-6701F, at 2KV) equipped with energy dispersive X-ray spectroscopy (EDX, Oxford), transmission electron microscopy (TEM, JEOL-2010, at 200KV) and high resolution TEM (HRTEM, JEOL-2010, at 200KV). X-ray photoelectron spectroscopy (XPS) measurements were carried out on a PHI 5000 instrument (Al Kα, $h\nu$ = 1486.7 eV) to examine the surface component and electronic structure. The elemental concentration of the samples was analyzed with an inductively coupled plasma-atomic emission spectroscopy (ICP-AES, Thermo, IRIS Advantage) for the catalysts used for the MOR evaluations.

2.3. Electrocatalytic evaluation towards MOR

The MOR evaluations were performed on an electrochemical workstation (VersaSTAT 4, AMETEK Princeton) with a rotating disk electrode system (RDE; ATA-1B, Jiangfen Instruments). A three-electrode cell configuration was used, including a platinum wire as counter electrode, an Hg/Hg_2SO_4 as reference electrode and a glass carbon (GC) electrode (A_{geom} = 0.196 cm^2) as working electrode. The GC electrode coated with the electrocatalyst ink was prepared similar to the method reported elsewhere [20,25]. The estimated loading of catalyst was ~20 $\mu g_{Pt} cm^{-2}$ for all cases.

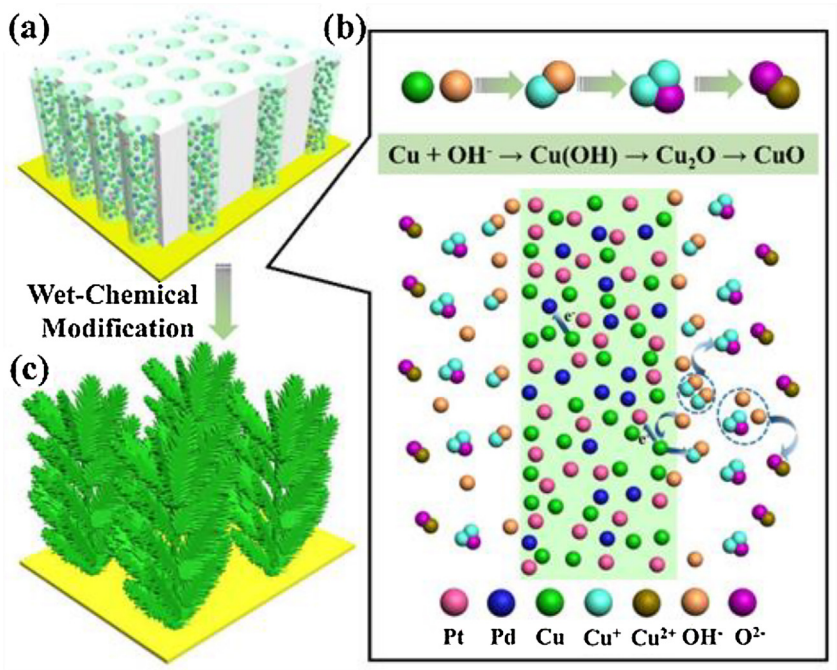

Fig. 1. Schematic illustration of the wet-chemical transformation of PtPdCu NWs into NDs. (a) The PtPdCu NWs obtained via AAO template-confined electrodeposition. (b) The galvanic cell reaction mechanism of PtPdCu NWs. (c) The hierarchical PtPdCu NDs achieved after being etched in 0.1 M HNO_3 when Cu atomic content is larger than 21.51 at%.

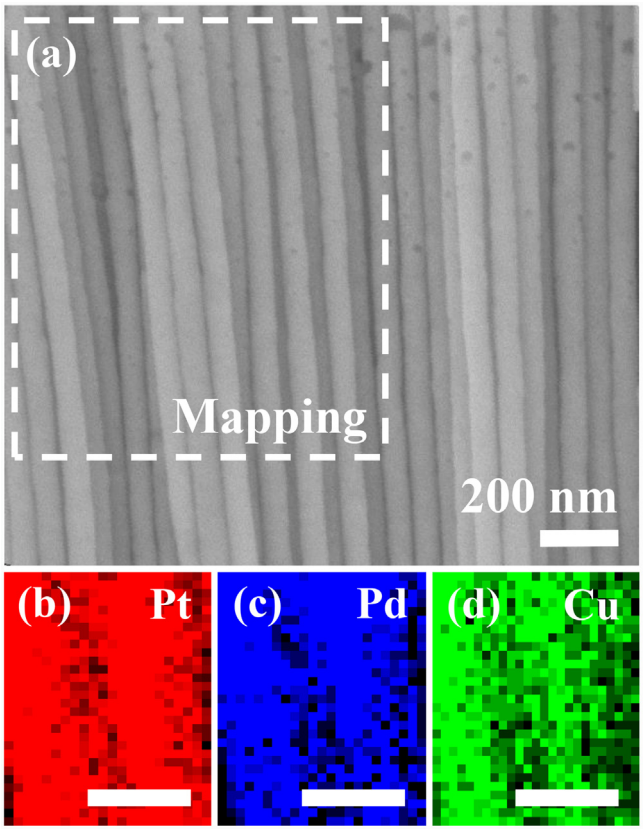

Fig. 2. (a) The SEM image of the PtPdCu NWs with the Cu atomic content of ~7.39 at%, achieved after being etched in 0.1 M HNO_3. The elemental mappings of Pt (b), Pd (c) and Cu (d) are taken from the dashed rectangle in (a), and all the scale bars are 500 nm.

All electrochemical measurements were performed at 25 °C, and the potential values were referenced to the reversible hydrogen electrode (RHE). After the catalysts-loaded electrode was activated in Ar-saturated 0.5 M H_2SO_4 by potential cycling between 0 V and 1.2 V at a sweep rate of 50 mVs^{-1} for 50 cycles, the cyclic voltammograms (CVs) and chronoamperometry (CA) curves towards MOR were recorded in 0.5 M H_2SO_4 + 1.0 M CH_3OH at 50 mVs^{-1}. Prior to the CO stripping measurements, high-purity CO (99.99% v/v in purity) was purged into the 0.5 M H_2SO_4 electrolyte for 15 min to obtain maximum coverage of CO on the Pt active sites. Then the dissolved CO was excluded by bubbling Ar gas (99.99% v/v in purity) for 20 min. Two consecutive CVs were recorded between 0 V and 1.2 V at 50 mVs^{-1}.

3. Results and discussion

3.1. Morphological and structural analysis

Fig. S1-3 (see the Supplementary material) show that after the AAO templates being totally dissolved, the pristine PtPdCu NWs without wet-chemical etching are cylindrical and uniform with smooth surface, and the diameter is around 70 nm. The corresponding Cu atomic content in the NWs is estimated ~ 44.87 at% by EDX analysis. After etching in 0.1 M HNO_3 for 1 h, the morphology of PtPdCu NWs arrays (Fig. 2a) does not change. The corresponding elemental mappings (Fig. 2b–d) reveal that the Pt, Pd and Cu elements distribute evenly along the longitudinal axis of the NWs, and the Cu atomic content is ~ 7.39 at% (Fig. S4, Supplementary material), with an atomic ratio of 9 (Pt):4 (Pd):1 (Cu). From further TEM, HR-TEM and selected area electron diffraction (SAED) characterizations (Fig. S5, Supplementary material), we observe that Pt, Pd and Cu atoms are homogeneously stacked with polycrystalline crystallization.

Interestingly, the morphology of the product can be tailored through tuning the electrodeposition parameters. For example, when the Cu content in the sample is increased, a large number of PtPdCu NDs (Fig. 3a), instead of NWs, with dense and irregular shapes are obtained. The corresponding elemental mappings (Fig. 3b–d) confirm that Pt, Pd and Cu elements are distributed homogeneously in the NDs. The magnified SEM images (Fig. 3e–f) clearly show the surface morphology of NDs composing of hierarchical tips and cracks. To understand the crystallization, a representative dendrite with tip-cracks is further investigated by TEM (Fig. 4a), from which the "dark contrast" in the middle as the "stems" and the "light contrast" in the edge as the "needles", respectively. The higher magnification TEM image (Fig. 4b) indicates that the "cracks" and "tips" surround the "needles", which might provide sufficient active sites for MOR (described below). Although the NDs are transforming from the NWs, their crystallinity is not destroyed. From the HR-TEM image (Fig. 4c), one can clearly identify that the Pt (111) plane and Pd (111) plane randomly arrange, and thus show polycrystalline in the SAED pattern (inset in Fig. 4c). The elemental mappings (Fig. 4d–f) further confirm that all elements are uniformly distributed in the flake configuration. From the EDX analysis (Fig. S6, Supplementary material), the atomic ratio is altered about 3 (Pt):3 (Pd):1 (Cu), and the Cu atomic content is ~ 21.51 at%.

The crystalline structures of catalysts are evaluated by XRD (Fig. S7, Supplementary material). In all cases, the typical face-centered cubic (*fcc*) structures are observed. All peak positions of Pt are consistent with standard Pt fcc crystalline (JCPDS No. 04-0802). However, the diffraction peaks of bimetallic PtPd and trimetallic PtPdCu catalysts are slightly shifted to higher 2θ angles compared with those of standard Pt. At the same time, the signals of pure Cu phases are not detected from the PtPdCu NDs catalysts, indicating the formation of single-phase alloys.

XPS analysis is further utilized to characterize the catalysts, and the Pt 4f spectra are shown in Fig. S8 in supplementary material. Compared to the Pt/C catalyst, a slight shift toward a lower binding energy of Pt 4f peak is observed for both PtPd NWs and PtPdCu NDs. Such shift indicates a modified electronic structure of Pt owing to the incorporation with Pd [26], which could contribute to better catalytic performance.

3.2. Synthesis mechanism of the PtPdCu NDs

Actually, the Cu content in PtPdCu nanostructures plays the vital role as intermediates in tailoring the dendritic shapes. Our systematic studies show that under the same experimental conditions, with a lower Cu atomic contents of ~7.39 at%, only NWs with nanopores on the surface were obtained (Fig. 2); while with the Cu atomic content reached to ~ 21.51 at%, tip-cracked NDs with hierarchical morphologies were achieved (Fig. 3). As to the reason of NWs-NDs morphologies transformation, it might be caused by the "galvanic cell" system which consists of Cu as the anode, Pt (or Pd) as the cathode, NaOH and HNO_3 as the electrolyte. In our cases, we take the NaOH electrolyte and the temperature (50 °C) as example. In such environment, Cu is first oxidized to form Cu_2O, and further oxidized into CuO [27,28]. The corresponding reaction can be illustrated as follows:

$$Cu + OH\bullet \rightarrow Cu(OH) + e\bullet \quad (1)$$

$$2Cu(OH) \rightarrow Cu_2O + H_2O \quad (2)$$

$$Cu_2O + 2OH\bullet \rightarrow 2CuO + H_2O + 2e\bullet \quad (3)$$

Hence, if a higher Cu content is used, a larger fraction of the Cu- Pt (Pd) "galvanic cells" takes place both inside the NWs and around

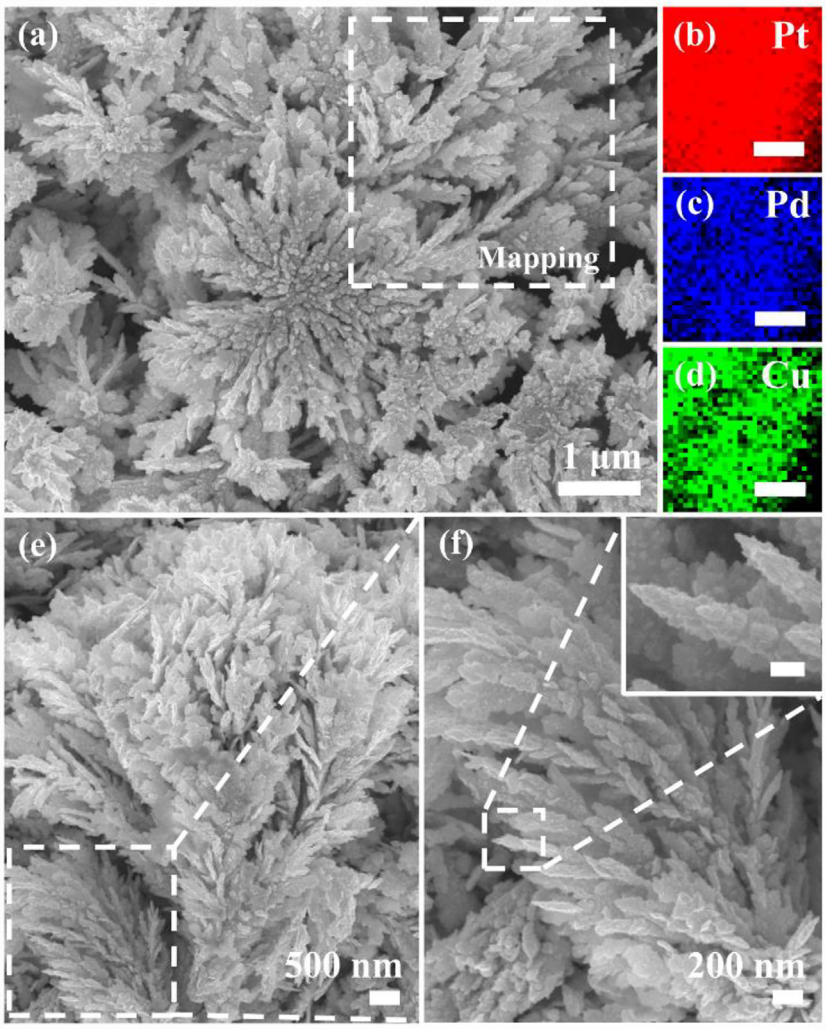

Fig. 3. (a) The SEM image of the hierarchical PtPdCu NDs achieved after being etched in 0.1 M HNO_3 with the Cu atomic content of ~21.51 at%. The elemental mappings of Pt (b), Pd (c) and Cu (d) are taken from the dashed rectangle of (a), respectively, and all the scale bars are 1 μm. (e)–(f) The SEM images taken by consecutive magnification, and the scale bar of inset in (f) is 100 nm.

the surface, forming the PtPdCu NDs (Fig. 3); while if a lower Cu content is employed, the "galvanic cells" only act around the NWs surface, forming the NWs with pores (Fig. 2).

3.3. Electrocatalytic performance of the PtPdCu NDs catalysts

We evaluate the electrocatalytic performance of tip-cracked PtPdCu NDs towards MOR, and with the commercial 20 wt% Pt/C (Fig. 5) and PtPdCu NWs (Fig. S9, Supplementary material) catalysts for comparison. The cyclic voltammograms (CVs) in red, black (Fig. 5a) and blue (Fig. S9a, Supplementary material) correspond to the PtPdCu NDs, Pt/C and PtPdCu NWs catalysts, respectively, from which all the curves display similar contours of hydrogen adsorption/desorption and the formation/reduction of Pt oxide. The actual electrochemical active surface area (ECSA) of Pt-based catalysts is generally calculated from the areas of hydrogen adsorption between 0.05 V and 0.4 V in the CVs. However, for multi-component alloys such as PtPd catalysts, the ECSA values are needed to be estimated integrating the CO stripping results (Fig. 6 and Fig. S11 in Supplementary material) due to the fact that the hydrogen adsorption peak from Pd might be appeared at the same potential range [26]. In our cases, the ECSA of PtPdCu NDs (59.6 m^2/g_{Pt}) calculated from the CO stripping voltammograms is ~ 1.42 times greater than that of the PtPdCu NWs (42.1 m^2/g_{Pt}), but is less than that of commercial Pt/C catalyst (71.5 m^2/g_{Pt}). The details of PtPdCu NWs are shown in Fig. S9 in Supplementary material.

The electrochemical activities of PtPdCu NDs catalyst towards MOR are investigated and compared with commercial Pt/C and PtPdCu NWs catalysts. The PtPdCu NDs exhibit electro-catalytic activity superior to that of Pt/C indicated by significant negative shift (135 mV) of MOR peak potential and higher peak current density. The CVs (Fig. 5b) show that the peak current density of PtPdCu NDs (688 mA/mg_{Pt}) is ~ 1.78 and ~ 1.49 times higher than those of Pt/C (386 mA/mg_{Pt}) and NWs (462 mA/mg_{Pt}, Fig. S9b, Supplementary material) catalysts, respectively, indicating that the PtPdCu NDs have a significantly higher mass activity towards MOR. When the activity is normalized to the ECSA, the specific peak current density (Fig. 5c) of PtPdCu NDs is ~ 1.154 mA/cm^2, which is ~ 2.14 times and ~ 1.05 times higher than those of Pt/C (~ 0.540 mA/cm^2) and PtPdCu NWs (~ 1.097 mA/cm^2, Fig. S9c, Supplementary material), respectively. Furthermore, the peak potential of the forward anodic peak of PtPdCu NDs catalyst (0.899 V) is also obviously lower than those of the PtPdCu NWs (0.950 V) and Pt/C catalysts (1.034 V), indicating that the PtPdCu NDs are easier to catalyze methanol oxidation. As a result, under equivalent Pt content, PtPdCu NDs perform better catalytic activity than those of PtPdCu NWs and commercial Pt/C.

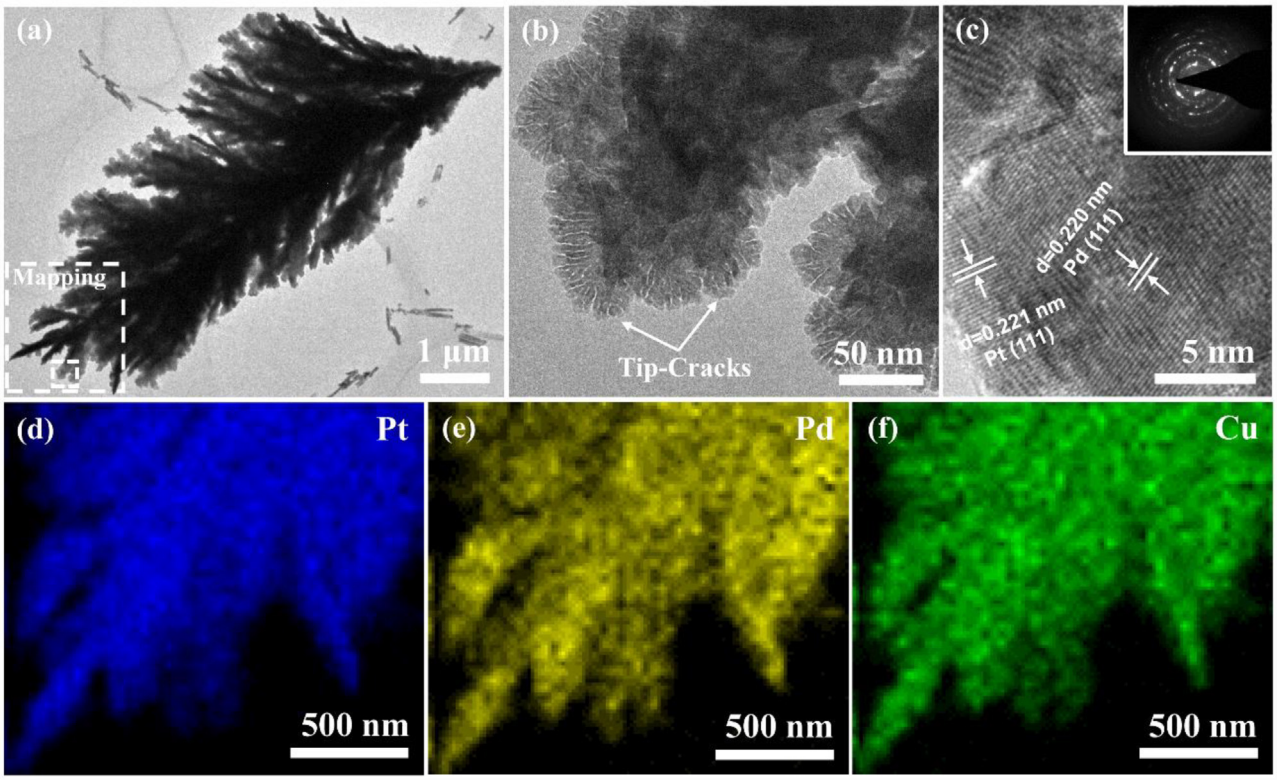

Fig. 4. The representative TEM image (a) and the enlarged TEM image (b) of the tip-cracked PtPdCu NDs achieved after being etched in 0.1 M HNO_3 with the Cu atomic content of ~21.51 at%. (c) The corresponding HR-TEM image is from (b). Inset SAED pattern is from (a). The elemental mappings of Pt (d), Pd (e) and Cu (f) are taken from the dashed rectangle of (a), respectively.

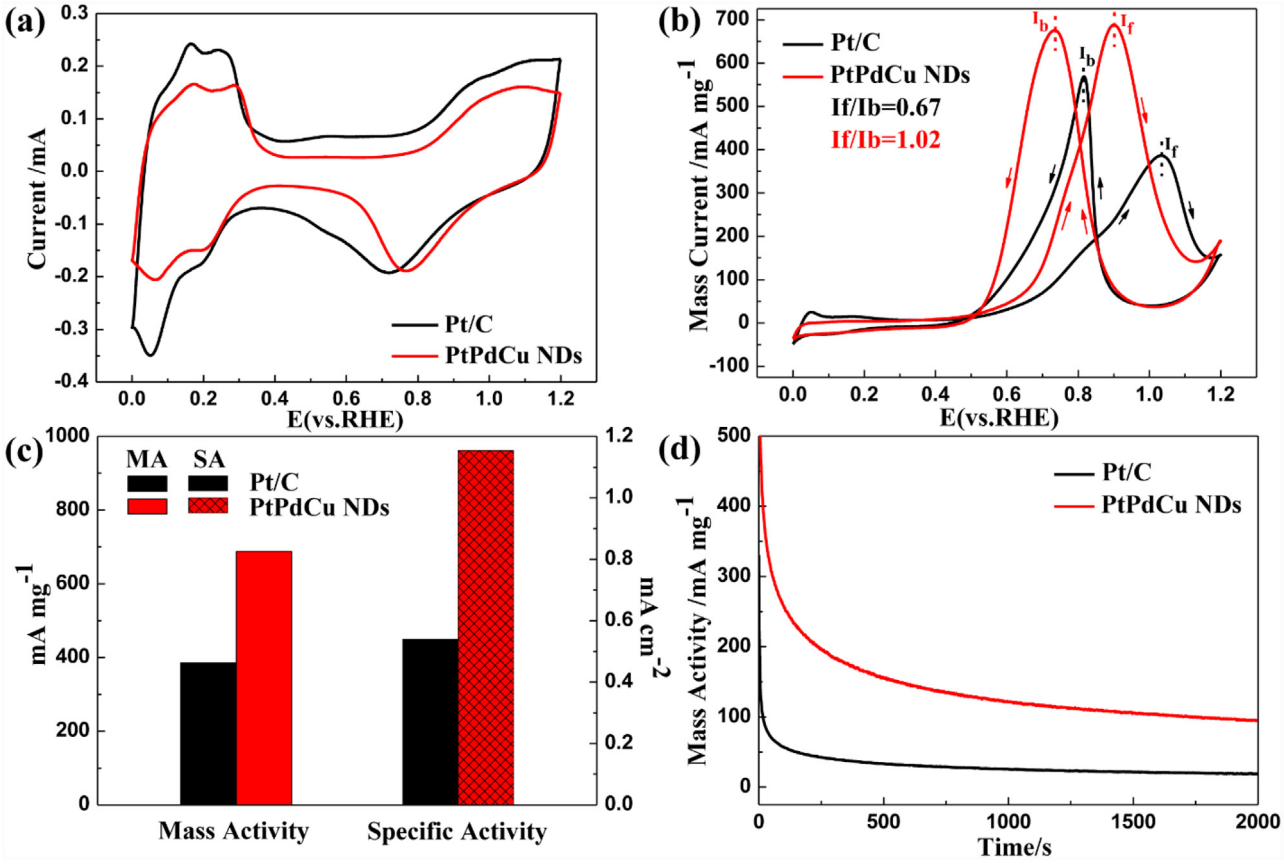

Fig. 5. The CVs of PtPdCu NDs and commercial Pt/C are obtained in (a) 0.5 M H_2SO_4 and in (b) 0.5 M H_2SO_4 + 1.0 M CH_3OH at 50 mVs^{-1}, respectively. (c) The mass activity and specific activity are corresponding to the PtPdCu NDs (red) and commercial Pt/C (black), respectively. (d) The CA curves are obtained in 0.5 M H_2SO_4 + 1.0 M CH_3OH at 50 mVs^{-1}. (For interpretation of the references to colour in this figure legend, the reader is referred to the web version of this article.)

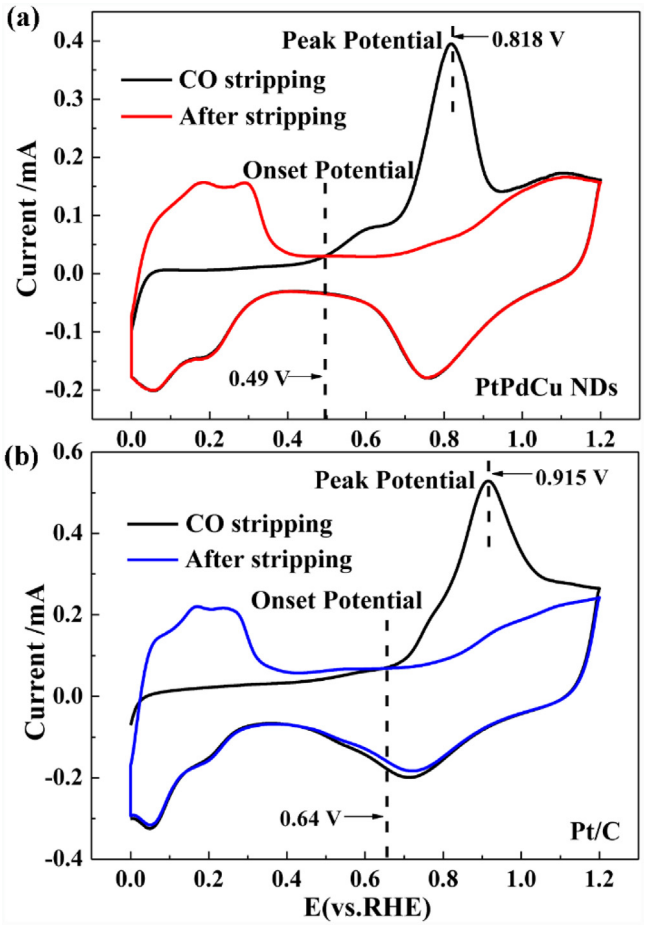

Fig. 6. The CO stripping measurements of (a) PtPdCu NDs and (b) commercial Pt/C catalysts in 0.5 M H_2SO_4 at 50 mV s^{-1}.

The ratio of the forward peak current to the backward one (I_f/I_b) is generally employed to evaluate the degree of oxophilicity [29,30]. In terms of I_f and I_b sharing the similar chemical origin of methanol oxidation, the less the Pt surface occupied with oxygenated species, the higher I_b is obtained, which implies that I_f/I_b is related to the degree of oxophilicity. In our cases, the I_f/I_b ratio of PtPdCu NDs (1.02) is ~1.10 and ~1.52 times higher than those of PtPdCu NWs (0.93) and commercial Pt/C (0.67), respectively, suggesting that tip-cracked PtPdCu NDs have higher oxopholicity (Fig. 5b and Fig. S9b in Supplementary material).

From the multiple CVs (Fig. S10, Supplementary material) of PtPdCu NDs and NWs, as well as commercial Pt/C catalysts with increasing cycle number, it is found that the catalytic activity of PtPdCu NDs remains almost stable with increasing cycle number, indicating better long-term stability towards MOR. By contrast, the mass current density of commercial Pt/C diminishes rapidly. Additionally, the PtPdCu NDs exhibit much higher catalytic activity than those of NWs and commercial Pt/C.

To further understand the stability of the electrocatalysts, CA curves are measured in 0.5 M H_2SO_4 + 1.0 M CH_3OH at 0.8 V for 2000 s (Fig. 5d and Fig. S9d in Supplementary material). Due to the poisoning caused by carbonaceous intermediate species, the current density decays sharply at the beginning and then undergoes a slow decrease. Clearly, the PtPdCu NDs exhibit a lower current deterioration rate than the PtPdCu NWs and Pt/C catalysts. Additionally, it is worth noting that the PtPdCu NDs exhibit a larger current density (94.77 mA/mg) after 2000s, which is ~1.86 times and ~5.02 times higher than those of PtPdCu NWs (50.99 mA/mg) and Pt/C (18.86 mA/mg), and thus hold the best activity and stability towards MOR among three samples.

As CO poisoning tolerance is an important indicator towards MOR, CO stripping measurements are performed to further evaluate the performance for CO anti-poisoning of the PtPdCu NDs catalyst. Two consecutive CVs are recorded for PtPdCu NDs (Fig. 6a), Pt/C catalyst (Fig. 6b) and PtPdCu NWs catalyst (Fig. S11, Supplementary material), respectively. The absence of hydrogen desorption peaks in the initial cycle (curves in black) is due to the monolayer adsorption of CO on the Pt surface. For all catalysts, a sharp peak appears during the first scan (black line) and disappears in the subsequent scan (red line), indicating that the adsorbed CO is completely oxidized during the first forward scan. Additionally, the onset potential of CO oxidation (indicated by the dashed line on the left) for the PtPdCu NDs (0.49 V) is much more negative than those for the PtPdCu NWs (0.61 V) and the commercial Pt/C (0.64 V) catalysts, indicating the easier removal of CO from the surface of PtPdCu NDs catalyst. On the other hand, the CO oxidation peak position (indicated by the dashed lines on the right) of PtPdCu NDs (0.818 V) is much lower than that of commercial Pt/C (0.915 V), indicating much better CO poising tolerance of the former. Interestingly, though PtPdCu NDs shows much lower onset potential for CO removal than that of PtPdCu NWs, it shows slightly larger peak potential (0.818 V) than that of the latter (0.786 V).

3.4. Roles of the crack tips and Pd dopants

In our cases, the enhancement in electrocatalytic performance towards MOR may be attributed to the synergistic effect generated from the NWs-NDs transformation and the Pd dopants. The "cracks" and hierarchical microstructures of NDs result in more rich atomic steps and more exposures of Pt and Pd atoms than those of PtPdCu NWs with smooth surface, which are highly favorable for maximizing the accessible surface area and obtaining more active sites. Additionally, Pd dopants are favorable to enhance the activity and the CO tolerance owing to the electronic effects [31] and bifunctional mechanism [1]. The modified electronic structure of Pt could effectively decrease the CO adsorption energy, facilitate the C—H cleavage on Pt sites and thus attribute to the shift of the d-band center [32,33], for which the NDs are more conducive to remove the CO from their surface than Pt/C catalyst. For the bifunctional mechanism, Pt is easier to carry out catalytic dehydrogenation of methanol to form Pt-CO, while the dissociation adsorption of H_2O molecules is more likely to occur on the Pd sites to form Pd-OH, which is favorable to promote the oxidation of CO to CO_2 at the same time to release the active site of Pt [34,35].

4. Conclusions

In summary, tip-cracked PtPdCu NDs have been developed via a combined synthetic route including AAO template-confined electrodeposition and subsequent wet-chemical modification, in which one-dimensional (1D) NWs with cylindrical and smooth surface are transformed into hierarchical NDs with surface-cracked shapes as the result of Cu attribution to galvanic cell reaction as intermediates. Owing to the synergetic effect between porous tip-cracked morphologies and Pd dopants, the as-synthesized PtPdCu NDs show significantly enhanced electro-catalytic activity and stability towards MOR compared with the PtPdCu NWs and commercial Pt/C catalysts. Moreover, the PtPdCu NDs display better CO tolerance than that of commercial Pt/C catalyst. Our approach for the fabrication of PtPdCu NDs might be applied to other materials, which could be obtained by first co-electrodeposition and subsequent wet-chemical modification. The achieved PtPdCu NDs hold great potential in DMFCs.

Acknowledgements

This work was financially supported by the Natural Science Foundation of China (Grant No. 21473093), Tianjin Research Program of Application Foundation and Advanced Technology (Grant No. 14JCYBJC41300) and Natural Sciences and Engineering Research Council of Canada (NSERC). The authors thank Prof. Fangyi Cheng (Nankai University, P. R. China), Prof. Weichao Wang (Nankai University, P. R. China), Prof. Dongsheng Geng (University of Science and Technology Beijing, P.R. China) and Prof. Zhenbo Wang (Harbin Institute of Technology, P.R. China) for the beneficial discussions on the MOR experimental evaluation.

Appendix A. Supplementary data

Supplementary data associated with this article can be found, in the online version, at http://dx.doi.org/10.1016/j.apcatb.2017.04.040.

References

[1] Z. Xiao, Y. Min, M. Liang, L. Liang, C. Liu, J. Liao, T. Lu, X. Wei, Energy Environ. Sci. 4 (2011) 2736–2753.
[2] R. Ganesan, J.S. Lee, Angew. Chem. Int. Ed. 44 (2005) 6557–6580.
[3] V. Stamenkovic, B.S. Mun, K.J.J. Mayrhofer, P.N. Ross, N.M. Markovic, J. Rossmeisl, J. Greeley, J.K. Nørskov, Angew. Chem. 45 (2006) 2897–2901.
[4] V.R. Stamenkovic, B.S. Mun, K.J.J. Mayrhofer, P.N. Ross, N.M. Markovic, J. Am. Chem. Soc. 128 (2006) 8813–8819.
[5] E. Casado-Rivera, D.J. Volpe, L. Alden, C. Lind, C. Downie, T. Vázquez-Alvarez, A.C. Angelo, F.J. Disalvo, H.D. Abruña, J. Am. Chem. Soc. 126 (2004) 4043–4049.
[6] O. Savadogo, K. Lee, K. Oishi, S. Mitsushima, N. Kamiya, K.I. Ota, Electrochem. Commun. 6 (2004) 105–109.
[7] H.H. Li, S. Zhao, M. Gong, C.H. Cui, D. He, H.W. Liang, L. Wu, S.H. Yu, Angew. Chem. Int. Ed. 52 (2013) 7472–7476.
[8] L. Wang, Y. Yamauchi, J. Am. Chem. Soc. 135 (2013) 16762–16765.
[9] S.S. Mahapatra, J. Datta, Int. J. Electrochem. 11 (2011) 155–169.
[10] N.P. Lebedeva, M.T.M. Koper, J.M. Feliu, R.A.v. Santen, J. Phys. Chem. B 106 (2002) 12938–12947.
[11] B. Hammer, J.K. Nørskov, Adv. Catal. 45 (2000) 71–129.
[12] D.Y. Chung, K.J. Lee, Y.E. Sung, J. Phys. Chem. C 120 (2016) 9028–9035.
[13] S.W. Lee, S. Chen, W. Sheng, N. Yabuuchi, Y.T. Kim, T. Mitani, E. Vescovo, Y. Shao-Horn, J. Am. Chem. Soc. 131 (2009) 15669–15677.
[14] G. García, M.T. Koper, Phys. Chem. Chem. Phys. 10 (2008) 3802–3811.
[15] G. García, A. González-Orive, M. Roca-Ayats, O. Guillén-Villafuerte, G. Á. Planes, M.V. Martínez-Huerta, A. Hernández-Creus, E. Pastor, Int. J. Hydrogen Energy (2016).
[16] B.W. Hao, Y.X. Bao, Y. Le, X.Y. Yu, W.L. Xiong, Nat. Commun. 6 (2015).
[17] S. Zhuo, J. Zhang, Y. Shi, Y. Huang, B. Zhang, Angew. Chem. 54 (2015) 5693–5696.
[18] D. Yang, L.F. Fonseca, Nano Lett. 13 (2013) 5642–5646.
[19] L.N. Zhang, H.H. Deng, F.L. Lin, X.W. Xu, S.H. Weng, A.L. Liu, X.H. Lin, X.H. Xia, W. Chen, Anal. Chem. 86 (2014) 2711–2718.
[20] G. Zhang, S. Sun, M. Cai, Y. Zhang, R. Li, X. Sun, Sci. Rep. 3 (2013) 1526.
[21] Z. Chen, M. Waje, W. Li, Y. Yan, Angew. Chem. Int. Ed. 46 (2007) 4060–4063.
[22] D. Yang, G. Meng, C. Zhu, X. Zhu, Chem. Commun. 46 (2009) 7110–7112.
[23] D. Yang, V. Luis, C. Jennifer, O. Wilfredo, R. Oscar, L.F. Fonseca, Small 9 (2013) 188–192.
[24] Z.L. Xiao, C.Y. Han, U. Welp, H.H. Wang, W.K. Kwok, G.A. Willing, J.M. Hiller, R.E. Cook, D.J.M. And, G.W. Crabtree, Nano Lett. 2 (2002) 1293–1297.
[25] S. Sun, G. Zhang, D. Geng, Y. Chen, R. Li, M. Cai, X. Sun, Angew. Chem. Int. Ed. 50 (2011) 422–426.
[26] Y.H. Cho, O.H. Kim, D.Y. Chung, H. Choe, Y.H. Cho, Y.E. Sung, Appl. Catal B 154–155 (2014) 309–315.
[27] H.H. Strehblow, B. Titze, Electrochim. Acta 25 (1980) 839–850.
[28] S.H. Xu, J. Mater. Chem. C 3 (2015) 2072–2079.
[29] A.M. Hofstead-Duffy, D.J. Chen, S.G. Sun, Y.Y.J. Tong, J. Mater. Chem. 22 (2012) 5205–5208.
[30] D.Y. Chung, K.J. Lee, Y.E. Sung, J. Phys. Chem. C 120 (2016) 9028–9035.
[31] E. Antolini, Energy Environ. Sci. 2 (2009) 915–931.
[32] D.Y. Wang, H.L. Chou, Y.C. Lin, F.J. Lai, C.H. Chen, J.F. Lee, B.J. Hwang, C.C. Chen, J. Am. Chem. Soc. 43 (2012) 10011–10020.
[33] Q. Fu, W.X. Li, Y. Yao, H. Liu, H.Y. Su, D. Ma, X.K. Gu, L. Chen, Z. Wang, H. Zhang, Science 328 (2010) 1141–1144.
[34] Y. Liu, M. Chi, V. Mazumder, K.L. More, S. Soled, J.D. Henao, S. Sun, Chem. Mater. 23 (2011) 4199–4203.
[35] B.A. Kakade, T. Tamaki, H. Ohashi, T. Yamaguchi, J. Phys. Chem. C 116 (2012) 7464–7470.